

A mineralogical reason why all exoplanets cannot be equally oxidising

Claire Marie Guimond,^{1*}† Oliver Shorttle,^{1,2} Sean Jordan,² John F. Rudge¹

¹*Department of Earth Sciences, University of Cambridge, Downing Street, Cambridge CB2 3EQ, UK*

²*Institute of Astronomy, University of Cambridge, Madingley Road, Cambridge CB3 0HA, UK*

Accepted XXX. Received YYY; in original form ZZZ

ABSTRACT

From core to atmosphere, the oxidation states of elements in a planet shape its character. Oxygen fugacity (f_{O_2}) is one parameter indicating these likely oxidation states. The ongoing search for atmospheres on rocky exoplanets benefits from understanding the plausible variety of their compositions, which depends strongly on their oxidation states—and if derived from interior outgassing, on the f_{O_2} at the top of their silicate mantles. This f_{O_2} must vary across compositionally-diverse exoplanets, but for a given planet its value is unconstrained insofar as it depends on how iron (the dominant multivalent element) is partitioned between its 2+ and 3+ oxidation states. Here we focus on another factor influencing how oxidising a mantle is—a factor modulating f_{O_2} even at fixed $\text{Fe}^{3+}/\text{Fe}^{2+}$ —the planet’s mineralogy. Only certain minerals (e.g., pyroxenes) incorporate Fe^{3+} . Having such minerals in smaller mantle proportions concentrates Fe^{3+} , increasing f_{O_2} . Mineral proportions change within planets according to pressure, and between planets according to bulk composition. Constrained by observed host star refractory abundances, we calculate a minimum f_{O_2} variability across exoplanet mantles, of at least two orders of magnitude, due to mineralogy alone. This variability is enough to alter by a hundredfold the mixing ratio of SO_2 directly outgassed from these mantles. We further predict that planets orbiting high-Mg/Si stars are more likely to outgas detectable amounts of SO_2 and H_2O ; and for low-Mg/Si stars, detectable CH_4 , all else equal. Even absent predictions of Fe^{3+} budgets, general insights can be obtained into how oxidising an exoplanet’s mantle is.

Key words: planets and satellites: interiors – planets and satellites: composition – planets and satellites: terrestrial planets

1 INTRODUCTION

Chemical redox equilibria are ubiquitous in all geologic systems. Through the transport of electrons, redox equilibria govern large-scale aspects of the rocky planets built on these systems: from the formation of iron cores (Wood et al. 2006; Elkins-Tanton & Seager 2008; Rubie et al. 2015; Lichtenberg 2021); to the production of magma (e.g., Holloway et al. 1992; Foley 2011; Stagno et al. 2013; Lin et al. 2021); the supply of volcanic gas, including greenhouse gases (e.g., Kasting et al. 1993; Delano 2001; Gaillard & Scaillet 2014; Ortenzi et al. 2020; Guimond et al. 2021; Liggins et al. 2022); and the availability of chemical species for synthesising biologic precursors and catalysing metabolic reactions (e.g., Muchowska et al. 2019; Wade et al. 2021). Thus the surface environments and atmospheres of rocky planets are profoundly influenced by how oxidising their interiors are. This concept, cemented early on (Kasting et al. 1993; Holland 2002; Kasting & Catling 2003), is now crucial to bear in mind as we

prepare to detect atmospheres on temperate rocky planets, and will hope to distinguish their possible biological origins from geological ones (Wordsworth et al. 2018; Wogan et al. 2020; Krissansen-Totton et al. 2021, 2022). The aim of this work is to test whether rocky exoplanets, which are expected to have diverse mantle compositions (Hinkel & Unterborn 2018; Putirka & Rarick 2019; Guimond et al. 2023; Spaargaren et al. 2023), will also have more or less oxidising mantles as a consequence.

1.1 Quantifying how oxidising a planet’s mantle is

The fugacity of a non-ideal gas like oxygen, O_2 , is the effective partial pressure it would have as an ideal gas with the same chemical potential. This seemingly abstract concept is a powerful tool for quantifying how reducing or oxidising a system is. O_2 appears in numerous redox equilibria in the interiors and at the surfaces of planets: both directly, e.g., in the homogeneous gas phase equilibrium $\text{H}_2 + \frac{1}{2} \text{O}_2 = \text{H}_2\text{O}$; and indirectly as metal oxides’ variable valence state, e.g., in the heterogeneous disproportionation equilibrium $3\text{FeO} = \text{Fe} + \text{Fe}_2\text{O}_3$ between three valence states of iron (Frost et al.

* Contact e-mail: claire.guimond@physics.ox.ac.uk

† Present address: University of Oxford, UK

2004; Frost & McCammon 2008). It is through the presence of such equilibria that the fugacity of oxygen (f_{O_2}) is constrained and can be quantified. This is possible *even when the system has no free O_2 phase*— f_{O_2} still remains a useful descriptor of how oxidising the system is, by representing the fictive partial pressure of an oxygen gas in equilibrium with the system.

The processes that influence f_{O_2} inside a planet are intrinsically linked to the oxidation of Fe, since—as a fact of stellar nucleosynthesis—Fe is by far the most abundant multivalent element found in rocky planets. Therefore, the distribution of Fe between its reduced and oxidised states is interconnected with f_{O_2} . We can illustrate this with an inside-out example for planets.

Hot and partially molten from the energy of accretion, a forming planet’s magma ocean might contain Fe co-existing in both its most reduced, metallic, form (Fe^0) and its ferrous oxide form (Fe^{2+}). The oxidation of iron metal to iron(II) oxide can be written as:



In our example, the activities, a , of Fe-metal and FeO (as dissolved species in the metal and magma phases respectively) would be inter-related with f_{O_2} through the equilibrium constant of (1):

$$K_{(1)} = \exp\left(\frac{-\Delta G^\circ}{RT}\right) = \frac{a_{\text{FeO}}}{a_{\text{Fe}}(f_{\text{O}_2})^{1/2}}, \quad (2)$$

where ΔG° is the Gibbs free energy of reaction (1) in J mol^{-1} , R is the gas constant in $\text{J mol}^{-1} \text{K}^{-1}$, and T is temperature in K. From the form of (2), it can be seen that for a system with magma and metal in equilibrium, this system will have higher f_{O_2} —be more oxidising—when there is proportionally more FeO in the magma (assuming for simplicity that the activity of FeO scales with its concentration).

For pure phases of Fe-metal and FeO in equilibrium, the activities in (2) would always be unity, offering just one possible f_{O_2} for a given temperature and pressure. Hence, the known f_{O_2} of equilibria such as (1)—the iron-wüstite (IW) buffer—are often used as reference values, wherein the f_{O_2} of a real system is reported as a difference from what this reference f_{O_2} would be at the temperature and pressure of interest.

In a natural system, estimating f_{O_2} requires knowing the activity of Fe-bearing components in each phase. Magma oceans are highly unlikely to be pure Fe metal and FeO in nature, and calculating these activities and thus absolute f_{O_2} , especially at high temperature and pressure, is non-trivial (e.g., Richter & Ghiorso 2012). We can see how this complication comes into the calculation of f_{O_2} by rewriting the activities in terms of the concentration of the species in the phase, X_i , and the rational activity coefficient, γ_i , which captures departure from ideality. For FeO in a magma from equilibrium (1):

$$a_{\text{FeO}}^{\text{magma}} = \gamma_{\text{FeO}}^{\text{magma}} X_{\text{FeO}}. \quad (3)$$

In this case, whilst X_{FeO} would be fixed by the overall amount of oxygen available, the rational activity coefficient may vary as a function of pressure, temperature, and the wider composition of the silicate melt. As a consequence, f_{O_2} in this scenario can change *even when the amount of oxygen is constant*; i.e., when $X_{\text{Fe}}/X_{\text{FeO}} = \text{constant}$.

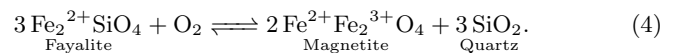
The above example makes the point that a complex natural system can become more or less oxidising independently of the amount of oxygen in it. This is true for solid systems of mineral equilibria, as much as for the liquid-liquid ‘core-forming’ equilibria looked at in reaction (1). It is these effects of activity on f_{O_2} that we investigate in this study, since they can be predicted independently of knowing the (hard to constrain) oxygen budget of the planet—which, simplistically, we consider here to be the ratio of Fe^{3+} to Fe^{2+} in a mantle rock.

1.2 Mantle mineralogy and f_{O_2}

The objective of this study is to calculate the effect of solid phase equilibria on mantle f_{O_2} for exoplanets of diverse composition. We are particularly concerned with the f_{O_2} at the top of an exoplanetary mantle: not only are the thermodynamic data better constrained at these lower temperatures and pressures ($\lesssim 25$ GPa; Guimond et al. 2023), but communication with the surface environment is more direct here. Magmas will likely be generated preferentially in the shallow mantle (as on Earth), and consequently, inherit its f_{O_2} , which will set the speciation of gases supplied to the atmosphere during volcanism (Gaillard et al. 2015; Ortenzi et al. 2020; Liggins et al. 2020; Guimond et al. 2021).

Whereas equilibrium (1) sets a mantle’s f_{O_2} during core formation, various subsequent mechanisms will likely move the mantle f_{O_2} away from this initial value (e.g., Frost et al. 2004; Wade & Wood 2005; Wood et al. 2006; Williams et al. 2012; Rubie et al. 2015; Hirschmann 2022). Through these processes, mantles can become oxidised such that iron exists between its 2+ (FeO) and its more oxidised 3+ (Fe_2O_3) valence states, as is the case for Earth’s mantle. The relevant equilibria setting how oxidising a mantle is, near its surface and some time after core formation, therefore involve minerals incorporating iron in these two oxidation states.

A useful reaction for illustrating this scenario is an equilibrium between the minerals olivine, spinel, and quartz. Here, iron can be present as FeO in olivine, as the component fayalite, and as a Fe_2O_3 component in spinel, called magnetite:



If olivine and spinel are solid-solution phases in equilibrium (4), f_{O_2} would be modulated upwards if either (i) the fayalite component in olivine is diluted by olivine’s other constituents (e.g., the forsterite component, Mg_2SiO_4); or (ii) the magnetite component is concentrated in spinel, independently of the amount of FeO or Fe_2O_3 . This is because concentration or dilution changes the activities of these components (3).

Like with the example of iron-wüstite reaction above, for the pure end-member phases, equilibrium (4) provides a commonly-used reference f_{O_2} , that of the fayalite-magnetite-quartz (FMQ) buffer. FMQ has an f_{O_2} close to that seen in Earth’s upper mantle, which is a coincidence resulting from Earth’s mantle’s composition (Earth’s mantle will not have quartz present).

Quartz is also not expected to be a common mineral in the shallow mantle mineralogies of many rocky exoplanets (Putirka & Rarick 2019; Guimond et al. 2023; Spaargaren et al. 2023). Rather, in most planets as on Earth, it is equi-

libria among olivine, pyroxenes, garnet, and spinel that set the f_{O_2} (see [Stolper et al. 2020](#), for a detailed review of these effects). The fact that these multi-mineral equilibria govern f_{O_2} means that the effect of shifting phase proportions on Fe_2O_3 activities will everywhere modulate the f_{O_2} of planetary mantles (e.g., [Frost 1991](#); [O’Neill et al. 1993](#); [Ballhaus 1995](#); [Rohrbach et al. 2007](#); [Frost & McCammon 2008](#); [Jennings & Holland 2015](#); [Stolper et al. 2020](#)). For Earth, this effect has been investigated in the context of an isochemical mantle (i.e., constant abundance ratio between all oxides, including FeO and Fe_2O_3) existing at different pressures, where order-of-magnitude changes in f_{O_2} were predicted just because of pressure-dependent mantle mineralogy ([Stolper et al. 2020](#)).

Beyond the solar system, however, mineral phase proportions at a given pressure will vary significantly according to the bulk mantle oxide proportions of a planet. This mineralogical effect on f_{O_2} can therefore be calculated for unknown exoplanets by modelling their plausible mineral phase equilibria, based on estimates of their bulk mantle metal oxide compositions, which, are expected to reflect the refractory element ratios observed in their host stars ([Anders & Ebihara 1982](#); [Thiabaud et al. 2015](#); [Bonsor et al. 2021](#)). In this way the chemical “star-planet connection” ([Hinkel & Unterborn 2018](#)) continues to be explored (e.g., [Unterborn et al. 2015](#); [Dorn et al. 2015, 2017a,b](#); [Santos et al. 2017](#); [Dorn et al. 2019](#); [Unterborn & Panero 2017, 2019](#); [Putirka & Rarick 2019](#); [Wang et al. 2019, 2022](#); [Otegi et al. 2020](#); [Spaargaren et al. 2020](#); [Spaargaren et al. 2023](#); [Guimond et al. 2023](#); [Unterborn et al. 2023, 2022](#)).

1.3 This study’s constraint on exoplanet mantle f_{O_2}

We cannot claim to know *a priori* the ratios of Fe^{3+} to Fe^{2+} in exoplanet mantles, which would be necessary to predict their absolute f_{O_2} . A more tractable endeavor is to fix the $\text{Fe}^{3+}/\text{Fe}^{2+}$ ratio at a nominal value for all planets, and calculate the *variability* of f_{O_2} due directly to phase equilibria; i.e., the changes in how Fe^{3+} is distributed between co-existing mineral phases and the impact of this on f_{O_2} . We go on to show that this variability is largely independent of the chosen $\text{Fe}^{3+}/\text{Fe}^{2+}$ ratio. By this method we hence produce an estimate of the minimum *variability* in mantle f_{O_2} across exoplanets: f_{O_2} must differ by *at least* this much because of mineralogy alone.

Because this f_{O_2} constraint is obtained from modelling mantle phase equilibria directly, our approach is complementary to previous work by [Ortenzi et al. \(2020\)](#) and [Liggins et al. \(2022\)](#), who explored the possibility of inferring mantle f_{O_2} from anticipated spectroscopic observations of exoplanet atmospheres—certain patterns of gas species in a volcanic atmosphere would in principle link to how oxidising the mantle source is. As for direct observational prospects, [Doyle et al. \(2019, 2020, 2023\)](#) report measurements of FeO abundances in planetary material at the end of its life, accreted in fragments onto white dwarfs. Such measurements would link to the bulk Fe oxidation state of the original parent body given an *a priori* estimate of how its iron inventory was partitioned between metal and oxides. Accurately retrieving parent body oxygen abundances from polluted white dwarfs remains difficult, however, as the perceived abundances can vary over time as material accretes ([Brouwers et al. 2023](#)).

We present a first *a priori* constraint on the variability of mantle f_{O_2} across exoplanets, stemming directly from refractory abundance distribution in the Hypatia Catalog of nearby stars ([Hinkel et al. 2014](#)). In section 2.1, we outline our method of calculating upper mantle mineralogy and the associated f_{O_2} from bulk mantle compositions, and in section 2.2, of converting from stellar refractory element abundances to these bulk mantle compositions. Section 3 presents the resulting distributions and various compositional correlations of f_{O_2} . Section 4 discusses a consequence for planetary evolution; namely, the speciation of outgassed volatiles. Section 5 concludes the study.

2 METHODS

2.1 Phase equilibria and oxygen fugacity

We use two independent models to calculate phase equilibria at pressures $P \in [1, 4]$ GPa, and temperature $T = 1373$ K, for a wide sample of hypothetical exoplanet bulk mantle compositions. Although we expect these two models to result in different values of absolute f_{O_2} —due to differences in how they incorporate Fe^{3+} into minerals and treat mineral solid solutions—we will show that the compositional variation in f_{O_2} is broadly robust to the choice of model. There are three components to each model: (i) the codes that solve for the stable mineralogy and mineral compositions; (ii) the thermodynamic databases, which contain data on endmember mineral component entropies, molar volumes, etc.; and (iii) activity-composition relations, or “mineral models”, that describe the solid solutions and their thermodynamics.

First, we use the pMELTS software package and its native thermodynamic database and mineral model ([Asimow & Ghiorso 1998](#); [Ghiorso et al. 2002](#)). For numerical stability, all calculations are initialised at superliquidus conditions, 2273 K. Then the system is cooled along the desired isobar in 5-K increments, until the T of interest is reached. The target temperature was chosen to be well below the solidus of typical rocky planet mantles. However, some mantles are predicted to still contain a small fraction of liquid, which will be having a small effect on the estimated f_{O_2} . We therefore exclude any mantle compositions with a remaining liquid phase in excess of 1 wt.% at the T of interest. About 50 compositions fail to converge at subsolidus temperatures with pMELTS and no stable phase assemblage can be found.

We perform a second set of calculations using the [Jennings & Holland \(2015\)](#) thermodynamic database and mineral model implemented in the code Perple_X ([Connolly 2009](#)); hereafter, JH-15. These calculations are done in the constrained minimisation mode of Perple_X, at the T and P of interest.

2.1.1 Pressures and mineral phases considered

Perple_X and pMELTS calculate the relative proportions of stable phases by minimising the Gibbs free energy for an input wt.% bulk oxide composition (section 2.2), over an input T and P . We consider cases where the solution phases olivine, orthopyroxene, clinopyroxene, spinel, and garnet comprise $\sim 100\%$ of the mineralogy between 1–4 GPa. We exclude any bulk compositions that stabilise a pure- SiO_2 phase (e.g.,

quartz, coesite) due to less-well-constrained thermodynamic data (see section 4.3.1). We further exclude the handful of compositions where pMELTS stabilises extraneous phases, such as kyanite or rhombohedral-oxide solution.

Our choice of pressure endpoints of 1 and 4 GPa excludes crustal phases whilst spanning the important spinel-garnet transition in the upper mantle. No subsolidus phase changes are expected at pressures between 4 and ~ 10 GPa for rocky exoplanet compositions (e.g., Guimond et al. 2023). Hence the mineral assemblages we calculate at 4 GPa should be representative of the bulk of the potential magma source region (Gaillard et al. 2021). Although we generally expect more reducing conditions at the higher pressures of the transition zone and lower mantle (Frost & McCammon 2008), we do not consider these mantle regions in our study: in part because the thermodynamic data is poorly-constrained, but also because these regions would not supply as much oxidising or reducing power to the planetary surface via magmatism.

We note that the hypothetical planet’s mass is not directly relevant for our calculations, given we are fixing T , P ; the only implicit constraint on planet mass therefore is that it be large enough to have mantles reaching 4 GPa (for context, Mars, 1/10 the mass of Earth, has a mantle pressure up to 19 GPa at its base; Stähler et al. 2021). The direct effect of planet mass in this framework is therefore just to change the depth in km corresponding to the pressure of interest. In practice, planet mass may have influenced the oxygen budget of the mantle (e.g., Frost & McCammon 2008; Deng et al. 2020), but such effects are not considered in this study.

2.1.2 Absolute oxygen fugacity from chemical potentials

The fugacity of O_2 is related to its chemical potential, μ , at the T and P of interest, relative to the standard state chemical potential, μ_0 , at 1 bar and the T of interest:

$$\log_{10} f_{O_2} = \frac{\mu - \mu_0}{RT \ln(10)}, \quad (5)$$

where $R = 8.3145 \text{ J mol}^{-1} \text{ K}^{-1}$ is the gas constant, and T is temperature in K. Thus by adopting a fixed T and P , we can perform meaningful comparisons of f_{O_2} between different bulk compositions.

The pMELTS software internally calculates $\log_{10} f_{O_2}$ at each T and P of interest (see Asimow & Ghiorsio 1998). Meanwhile, Perple_X only returns μ , so here we explicitly use (5) to find $\log_{10} f_{O_2}$, with μ_0 calculated via the same JH-15 database.

2.1.3 Relative oxygen fugacity using buffers

Because oxygen fugacities strongly depend on T and (less so) P , it is convenient to report them as a difference in dex with respect to the value of $\log_{10} f_{O_2}$ produced by a known buffer reaction—such as (1) or (4)—at the same T and P of interest. For relatively modest changes in T and P , intrinsic $\log_{10} f_{O_2}$ differences between system and buffer will be approximately preserved, thus largely normalising out the direct effect of temperature on $\log_{10} f_{O_2}$. Hence we will also report most of our calculations as a relative $\log_{10} f_{O_2}$ with respect to FMQ (4), denoted ΔFMQ .

We calculate $\log_{10} f_{O_2}$ of FMQ using JH-15, and subtract the absolute $\log_{10} f_{O_2}$ from pMELTS or JH-15 to find

ΔFMQ . We emphasise, however, that the ΔFMQ values we find are not the key result here, rather their distribution.

2.2 Mantle bulk composition from stellar element abundances

Our method of converting stellar abundances to phase proportions is essentially the same as in Guimond et al. (2023) and discussed there in more detail.

We take the entire sample of planet-hosting FGKM stars from the Hypatia Catalog (Hinkel et al. 2014) which have measured Mg, Si, Fe, Ca, Al, Na, and Ti, using the reported mean if a star has been measured more than once. Here, the normalised stellar abundance of an element X with respect to hydrogen is reported as:

$$[X/H] = \log_{10}(n_X/n_H)_* - \log_{10}(n_X/n_H)_\odot, \quad (6)$$

where n is the number abundance, the subscript $*$ denotes the value for the star, and the subscript \odot denotes the solar value from Lodders et al. (2009). We conserve the relative number abundances of Mg, Si, Fe, Ca, Al, Na, and Ti between the star and the bulk planet.

Within planet interiors, these seven elements together with oxygen will occur as component oxides (e.g., MgO, SiO₂) of mantle mineral phases, which constitute virtually its entire mass. We place most of the bulk Fe as a metallic planetary core, leaving an unconstrained but minority fraction as Fe oxide in the mantle. That is, we assume that there is enough O available to bond with all of the Mg, Si, Ca, Al, Na, and Ti; we do not track the affinity of O for rocky or volatile/icy material in the protoplanetary disc. Because the extent of Fe oxidation is unknown *a priori*, we use a free parameter $\chi_{\text{Fe}}^{\text{mantle}} = \text{Fe}_{\text{mantle}} / (\text{Fe}_{\text{core}} + \text{Fe}_{\text{mantle}})$ which defines the molar ratio of FeO* in mantle oxides to the total bulk planet Fe—here and throughout we use FeO* to mean the sum of iron oxides regardless of the valence state of iron (2+ or 3+), whilst FeO denotes ferrous iron oxide alone. We initially use a fixed value of $\chi_{\text{Fe}}^{\text{mantle}} = 0.12$ (that reproduces Earth’s core mass fraction for pure, solid Fe), but later test the effects of varying $\chi_{\text{Fe}}^{\text{mantle}}$ on the distribution of f_{O_2} .

To find the bulk composition of the mantle in weight percent, being the required input to the thermodynamic models, we convert the abundance of each element $[X/H]$ to its wt.% equivalent, conserving the total moles of Fe as described in Guimond et al. (2023, n.b. here we interpret their FeO as FeO*).

Planetary mantles will only inherit their host star $[X/H]$ if element X is perfectly refractory. Ca, Al, Mg, Si, Fe, and Ti are highly refractory, so we apply our stellar abundance-to-mantle oxide method at face value (but removing some Fe to the core as above). For Na, which is more volatile, as a first guess we approximate a depletion factor: we calculate the molar ratio of Na/Ti in the bulk silicate Earth (Workman & Hart 2005) relative to Na/Ti in the solar photosphere (Lodders et al. 2009), and scale $[Na/H]$ by this constant planet/star depletion factor of 0.046 across all systems. Spaargaren et al. (2023), in a similar attempt to relate stellar to planetary compositions, additionally account for possible Si in the core and for the slightly higher volatility of Mg versus Si, and hence produce slightly different Mg/Si ratios than our model. The effects of secondary processing on mantle Mg/Si ratios do not

affect our f_{O_2} variability results, but are briefly discussed in 4.3.

The bulk mantle compositions resulting from this method will be approximations of the true composition of a planet; caveats are discussed more extensively in Guimond et al. (2023). However, because it allows us to cover a large sample (>1000) of observed stellar compositions, our approach can provide a useful estimate of the corresponding breadth of mineralogically-driven f_{O_2} variation, regardless of the true median, which is in any case beyond our reach.

2.2.1 Nominal ferric iron content

To calculate f_{O_2} emerging from Fe redox equilibria, we must specify, as thermodynamic components in the system, either FeO^* and O_2 (Perple_X input), or FeO and Fe_2O_3 (pMELTS input). Both ways of describing the composition of the system are equivalent, as some amount of nominal O_2 in fact forms ferric iron to create a unique molar ratio of FeO to Fe_2O_3 (again, assuming no other multivalent, redox-active elements are present in the system). From the stoichiometry of the simple redox reaction $4\text{FeO} + \text{O}_2 \rightleftharpoons 2\text{Fe}_2\text{O}_3$, we have 2 mol Fe_2O_3 for every mol O_2 , and 2 mol Fe^{3+} for every mol Fe_2O_3 , so the effective molar abundance of O_2 is:

$$n_{\text{O}_2} = \frac{1}{4} (\text{Fe}^{3+}/\Sigma\text{Fe}) n_{\text{FeO}^*}, \quad (7)$$

where $\text{Fe}^{3+}/\Sigma\text{Fe}$ is the molar ratio of ferric iron to total iron in the (bulk) mantle, and n_{FeO^*} is the molar abundance of Fe in mantle oxides as required by stellar element abundances and $\chi_{\text{Fe}}^{\text{mantle}}$.

Equivalently, we can find the component mass fractions of FeO and Fe_2O_3 by simultaneously solving:

$$\text{Fe}^{3+}/\Sigma\text{Fe} = \frac{2m_{\text{Fe}_2\text{O}_3}/M_{\text{Fe}_2\text{O}_3}}{m_{\text{FeO}}/M_{\text{FeO}} + 2m_{\text{Fe}_2\text{O}_3}/M_{\text{Fe}_2\text{O}_3}} \quad (8)$$

$$m_{\text{FeO}^*} = m_{\text{FeO}} + m_{\text{Fe}_2\text{O}_3},$$

where m denotes the mass in kg and M the molar mass in kg mol^{-1} for the subscripted species.

In this way, a fixed $\text{Fe}^{3+}/\Sigma\text{Fe}$ is imposed across all compositions: for Perple_X runs O_2 is added to make up the required $\text{Fe}^{3+}/\Sigma\text{Fe}$ given FeO^* using (7); or, for pMELTS runs, FeO^* is divided into FeO and Fe_2O_3 using (8). Note that in either case the total mass or number amount drops out once the bulk composition is re-normalised to 100%. Earth's mantle $\text{Fe}^{3+}/\Sigma\text{Fe}$ value of 3% would be equivalent to having 8.2 wt.% FeO react with 0.027 wt.% O_2 .

Note that different choices of $\text{Fe}^{3+}/\Sigma\text{Fe}$ will have a minor effect on equilibrium mineralogy. Increasing $\text{Fe}^{3+}/\Sigma\text{Fe}$ from 3% to 10%, for example, increases the amount of orthopyroxene by a few wt.% at the expense of clinopyroxene. However, the amount of mineralogically-derived variability in mantle f_{O_2} is roughly preserved across different values of $\text{Fe}^{3+}/\Sigma\text{Fe}$, as we will show.

2.2.2 Choice of oxide components

The major rock-forming oxides MgO , SiO_2 , CaO , Al_2O_3 , and FeO^* should make up > 99% of exoplanetary mantles by mass—considering only these components would suffice if our only goal were to estimate phase abundances. However, other minor oxides can potentially have a non-negligible influence

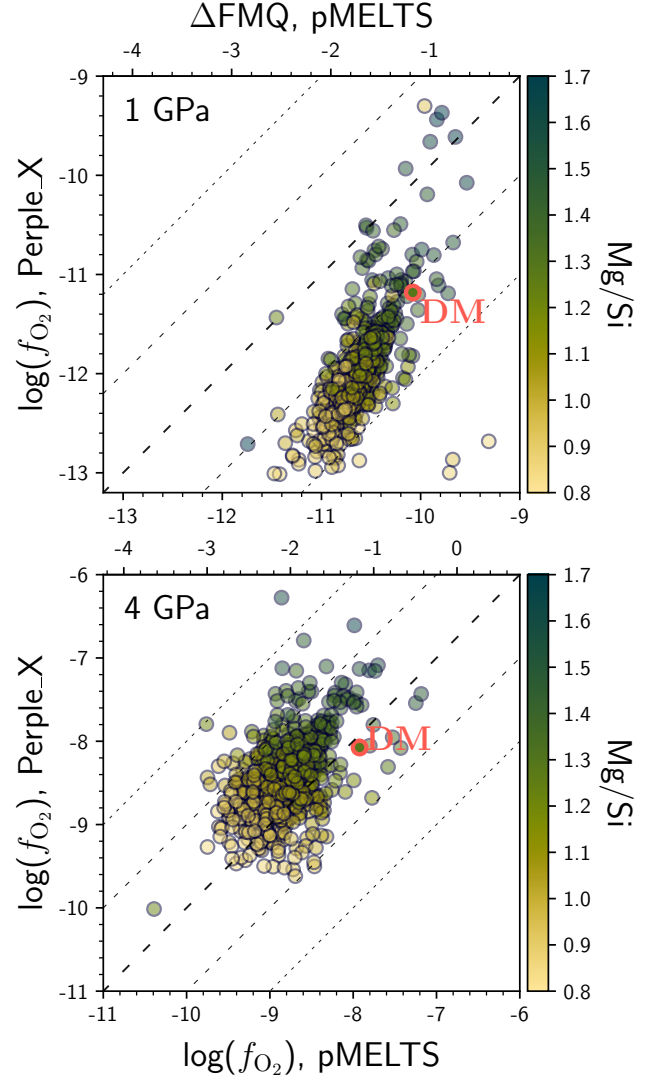


Figure 1. Direct comparison of absolute f_{O_2} between the pMELTS and JH-15 in Perple_X models, at 1 GPa (top) and 4 GPa (bottom) and 1373.15 K. Each point represents the bulk mantle composition inferred from a planet-hosting star in the Hypatia Catalog, assuming $\text{Fe}^{3+}/\Sigma\text{Fe} = 3\%$ and $\text{Fe}_{\text{mantle}}/(\text{Fe}_{\text{core}} + \text{Fe}_{\text{mantle}}) = 12\%$. Earth's depleted mantle (DM) composition from Workman & Hart (2005) is highlighted in red for comparison. Points are coloured by the molar Mg/Si ratio. Both models' compositions are in terms of MgO , SiO_2 , Al_2O_3 , CaO , Na_2O , Cr_2O_3 , FeO , and Fe_2O_3 ; pMELTS has TiO_2 in addition.

on mantle f_{O_2} , either by stabilising important ferric iron-hosting phases at different T, P , or affecting Fe^{3+} substitution in crystal structures. Hence, as in Stolper et al. (2020), we also consider Na_2O and TiO_2 , and in one set of reference calculations, Cr_2O_3 .

Although the presence of Na_2O has minor effects on orthopyroxene phase proportions in both pMELTS and JH-15 (changing them by $\lesssim 10$ wt.%), this can lead to disproportionately large effects on f_{O_2} . Including TiO_2 in the pMELTS runs is necessary to ensure that numerically-stable subsolidus phase assemblages can be found for most bulk compositions. Meanwhile, JH-15 can only place TiO_2 in a pure rutile phase,

so for `Perple_X` runs we exclude TiO_2 from bulk compositions in the thermodynamic modelling, although we still retrieve stellar Ti to calculate the Na depletion as discussed above. Minor amounts of Cr_2O_3 affect Fe^{3+} substitution into pyroxenes, whilst stabilising spinel at slightly higher pressures, allowing Earth’s upper mantle f_{O_2} to be reproduced more accurately from Earth’s depleted mantle composition.

3 RESULTS

3.1 The host minerals of ferric iron in planetary mantles

JH-15 and pMELTS model the thermodynamics of ferric iron incorporation into mineral phases as particular Fe^{3+} -bearing mineral endmembers. The models differ in the endmembers they use, their solution models, and the thermodynamics of those solution models. From this fundamental description of the minerals emerges partitioning behaviour of Fe^{3+} (and other elements). These important differences in how the models we use are constituted leads to systematically different absolute f_{O_2} between them for a given bulk composition, sometimes by 2 dex (Figure 1). So not only is predicting f_{O_2} hard for a planetary mantle without prior knowledge of its ferric iron abundance, it is challenging even when we can assume its ferric iron abundance. However, we will show that between the two models we use, (i) the amount of f_{O_2} variation is similar, and (ii) the compositional dependence of the f_{O_2} variation is also similar. As we are focusing on f_{O_2} variability arising from changes in bulk mantle composition, the fact that the models agree on this suggests the ensuing insights are robust.

The main phenomenon causing f_{O_2} to vary for constant bulk mantle $\text{Fe}^{3+}/\Sigma\text{Fe}$ is that different minerals partition characteristically different amounts of ferric iron into their crystal structures. We illustrate this phenomenon with a series of ternary diagrams (Figure 2), showing Fe_2O_3 modality for each bulk composition inferred from our Hypatia sample, to better understand the origins of the f_{O_2} variations produced by pMELTS and JH-15. Ternary diagrams are useful for plotting three variables which sum to unity, as is the case here.

At 1 GPa, the stable phases that incorporate Fe^{3+} are orthopyroxene, clinopyroxene, and spinel (note an olivine phase is almost always present yet contains no Fe^{3+}). Each point in the top row of Figure 2 shows the mass fraction of Fe_2O_3 in those phases for a given mantle composition, weighted by the mass fraction of the phase itself in the system. The fact that most points plot near the bottom-right corner shows that orthopyroxene is the most important Fe^{3+} host in almost all compositions at 1 GPa, for both models. Although spinel’s crystal structure may incorporate higher fractions of Fe^{3+} , when spinel is stable, its overall abundance rests at a few percent, and so has limited scope to affect the local f_{O_2} . In fact, the JH-15 model produces some mineralogies with very small spinel abundances, so many points in the top right panel of Figure 2 plot very close to the right edge of the diagram ($\sim 0\%$ spinel axis).

At 4 GPa—bottom row of Figure 2—spinel has been replaced by garnet, which has different Fe^{3+} partitioning behaviour. Further, unlike spinel, garnet can start to form

sizeable proportions of the mantle at a few GPa, especially for the more Al-rich planetary compositions. In the JH-15 model, orthopyroxene exchanges Fe^{3+} with garnet (although not shown, more Fe^{3+} partitions into garnet with increasing P). Meanwhile, the pMELTS model does not place Fe^{3+} into garnet, hence all points in the bottom left panel of Figure 2 plot on the $\sim 0\%$ garnet axis.

Note that in order to reproduce the Earth’s present-day upper mantle (“depleted mantle”) f_{O_2} near to FMQ, the calculations in Figure 1 included Cr_2O_3 in the bulk compositions. The presence of the minor cation Cr^{3+} can significantly influence Fe^{3+} partitioning (even without affecting modal mineralogy; see section 2.2). However, all subsequent calculations omit Cr_2O_3 because (i) Cr is moderately volatile (hence less-related to the stellar abundance), and (ii) Cr measurements are less-frequently listed in the Hypatia stellar compositions ($N = 636$ in the Figure 1 sample). The deceptively large effect of minor cations on f_{O_2} highlights the fact that absolute f_{O_2} , along with being model-dependent, cannot be constrained precisely without detailed compositional information. For example, the depleted mantle composition in Figure 1 would be 1 log unit more oxidised without Cr in the pMELTS model at 1 GPa.

3.2 Compositional correlations of f_{O_2}

Given that the majority of Fe_2O_3 is in orthopyroxene for most planetary mantle compositions (Figure 1) and the proportion of Fe_2O_3 in olivine is always zero, it follows that the main predictor of upper mantle f_{O_2} for a given $\text{Fe}^{3+}/\Sigma\text{Fe}$ would be the olivine/orthopyroxene ratio. A greater olivine/orthopyroxene ratio concentrates the mantle’s Fe^{3+} budget into orthopyroxene, thus raising the activity $a_{\text{Fe}_2\text{O}_3}^{\text{opx}}$ (compare (2)). The olivine/orthopyroxene ratio will be itself strongly positively correlated with Mg/Si (Hinkel & Unterborn 2018; Spaargaren et al. 2023; Guimond et al. 2023), a fact of these phases’ chemical stoichiometries: the Mg-endmember of olivine Mg_2SiO_4 (forsterite) requires 2 atoms of Mg per atom Si, while the Mg-endmember of orthopyroxene MgSiO_3 (enstatite) requires 1 atom Mg per atom Si. Thus, excess Mg with respect to Si builds olivine-dominated mineralogies. Magnesium and silicon have this dominant role in setting planetary mineralogy simply because of their high cosmochemical abundance.

Figures 3 and 4 show the relationship between f_{O_2} (as ΔFMQ) and Mg/Si, plus various other parameters describing bulk planet composition, for pMELTS and JH-15 respectively. A key result is that despite the differences between the two models (section 2.1), they nonetheless predict fundamentally similar systematics between f_{O_2} and planetary parameters. We emphasise that $\text{Fe}^{3+}/\Sigma\text{Fe}$ and thus the real f_{O_2} is unconstrained for exoplanets; we fix $\text{Fe}^{3+}/\Sigma\text{Fe}$ at 3% for the sake of creating these figures. The Mg/Si effect that we have explained in the previous paragraph induces ~ 3 orders of magnitude variation in mantle f_{O_2} (left-most columns). The scatter in f_{O_2} versus Mg/Si at 1 GPa is wider due to slightly more complicated phase equilibria at the lower pressures; pMELTS further places more Fe^{3+} into spinel, with more scope for affecting f_{O_2} (Figure 2). We find that the correlation of ΔFMQ with Mg/Si at 1 GPa has a slope of 1.4 and 3.0, in pMELTS and JH-15 respectively, and at 4 GPa, 3.4 and 4.0 (Supplementary Figure S1).

The relationship between Al/Si and f_{O_2} is more complex

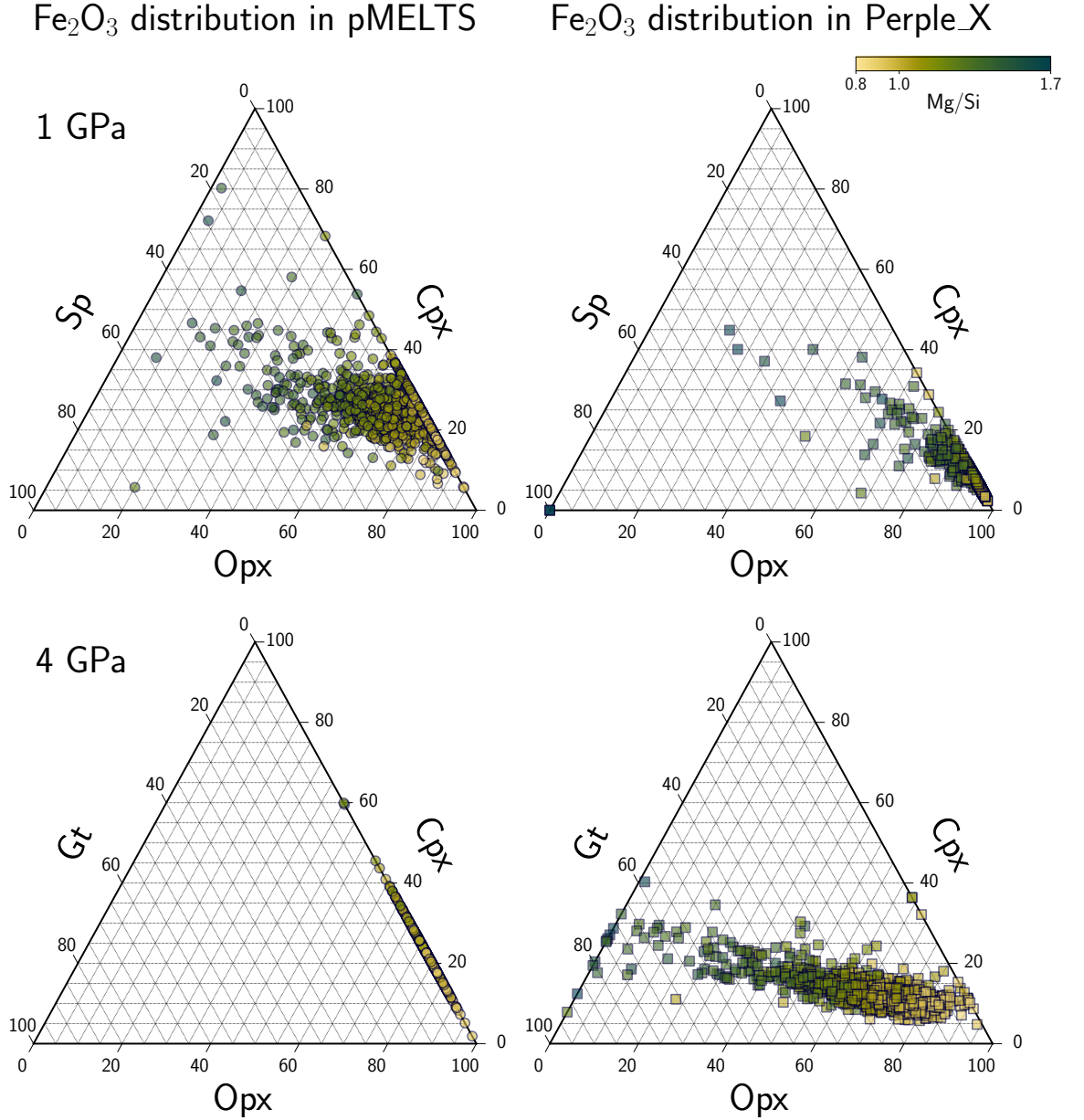


Figure 2. Ternary diagram showing the distribution (modality) of Fe_2O_3 between its subsolidus host phases: orthopyroxene (Opx), clinopyroxene (Cpx), and spinel (Sp) or garnet (Gt), at 1 GPa (*top*) and 4 GPa (*bottom*) and 1373.15 K. Olivine contains no Fe^{3+} in either of the thermodynamic databases we consider. Fe_2O_3 modality is calculated as the weight fraction of Fe_2O_3 in each phase, multiplied by the phase's total weight fraction in the system, and normalised to 100% between the three phases on each axis. The right column shows results from pMELTS, and the left column shows Perple_X results. Each point represents a bulk mantle composition (Ca-Na-Fe-Mg-Al-Si-O, plus Ti in pMELTS) inferred for a planet-hosting star in the Hypatia Catalog. Points are coloured by Mg/Si. Note that the horizontal guides correspond to the Cpx axis.

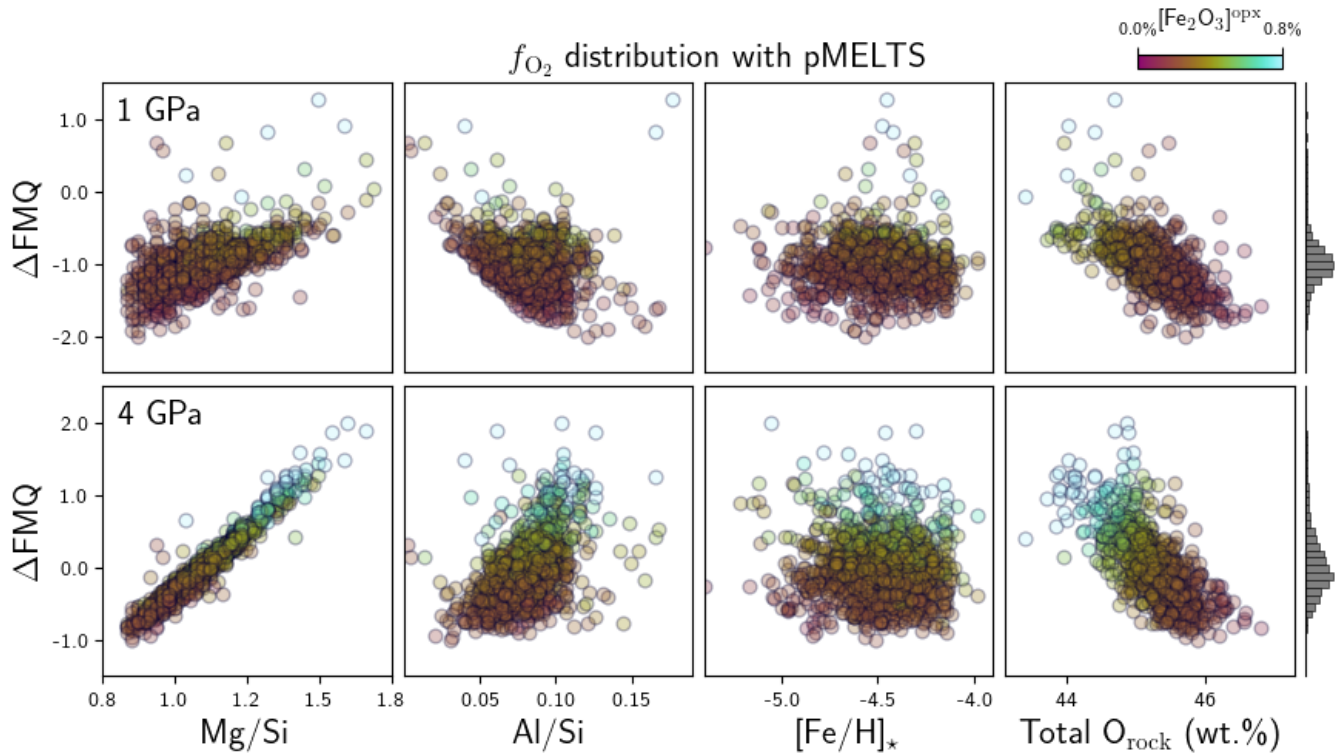


Figure 3. Cross plots of $\log(f_{\text{O}_2})$ expressed as ΔFMQ , resulting from pMELTS calculations, shown at 1 GPa (*top*) and 4 GPa (*bottom*) and 1373.15 K. From left to right, columns show the dependence of ΔFMQ on bulk mantle Mg/Si, Al/Si, stellar metallicity $[\text{Fe}/\text{H}]_*$, and the total refractory oxygen present in the mantle, O_{rock} (i.e., a sum over oxygen in all metal oxides). Each point ($N = 1198$) represents a bulk mantle composition (Ca-Na-Fe-Mg-Al-Si-O-Ti) inferred for a planet-hosting star in the Hypatia Catalog, assuming $\text{Fe}^{3+}/\Sigma\text{Fe} = 3\%$ and $\text{Fe}_{\text{mantle}}/(\text{Fe}_{\text{core}} + \text{Fe}_{\text{mantle}}) = 12\%$. Points are coloured by the Fe_2O_3 wt.% composition of orthopyroxene (opx). Histograms of the ΔFMQ distribution are projected on the y -axis.

(Figures 3 and 4, second columns), but again consistent between models. In pMELTS and JH-15 the correlation with f_{O_2} is negative in the spinel field, yet positive in the garnet field. Several effects lead to this behaviour and are discussed more thoroughly in Stolper et al. (2020). Most directly, Al-rich compositions stabilise mantles with higher proportions of the aluminous phases spinel and garnet, and less pyroxene (Supplementary Figure S2). In pMELTS at high pressure, where garnet does not take any Fe^{3+} , the Fe_2O_3 activity in orthopyroxene therefore increases with increasing Al/Si. In JH-15, Fe^{3+} is redistributed between garnet and orthopyroxene, so the trend is less straightforward and the correlation between f_{O_2} and Al/Si becomes weaker. Similarly at 1 GPa, larger proportions of spinel dilute the Fe^{3+} -bearing component in this aluminous phase, which can have a bearing on f_{O_2} .

The third columns of Figures 3 and 4 demonstrate how no correlation exists between upper mantle f_{O_2} and stellar Fe abundance (metallicity, $[\text{Fe}/\text{H}]_*$), at a fixed molar distribution of planetary iron between $\text{Fe}^0/\text{Fe}^{2+}/\text{Fe}^{3+}$. Increasing the total Fe in planetary mantles does not significantly affect the partitioning of ferric iron between minerals in pMELTS and JH-15; the ratios of Fe_2O_3 and FeO activities in host minerals are largely independent of total Fe.

Lastly, in the fourth columns, we show the correlation between f_{O_2} and the total mass percent of refractory oxygen

bound as metal oxides (e.g., O in SiO_2 , CaO etc.), which we call the total O_{rock} (wt.%). Both models show that total O_{rock} is strongly negatively correlated with mantle f_{O_2} at both pressures. This seemingly counter-intuitive negative correlation is a stoichiometric effect aliasing the Mg/Si effect above; it arises from the valence state of the metal oxides forming the planet’s mantle. As Mg occurs as MgO and Si as SiO_2 , higher Mg/Si favours forsterite (Mg_2SiO_4), which is 45.5% O by mass, over enstatite (MgSiO_3), which is 47.8% O by mass. Because planets with higher Mg/Si will have higher ratios of forsterite to enstatite, they will therefore have lower total O_{rock} for stoichiometric reasons, whilst having higher f_{O_2} for thermodynamic reasons. Further discussion of the Mg/Si ratio’s effect on the amount of refractory O that condenses to form planets can be found in Unterborn & Panero (2017).

3.3 Minimum variability of f_{O_2} across mantle compositions

The previous subsections set up an understanding of the f_{O_2} variability caused by changing mineral proportions in the upper mantles of rocky exoplanets. We call our distributions a minimum variability because observations of exoplanet host star chemistry imply that these mineralogies should indeed vary across exoplanets (Hinkel et al. 2014; Putirka & Rarick 2019). The true variability of f_{O_2} will be broader than

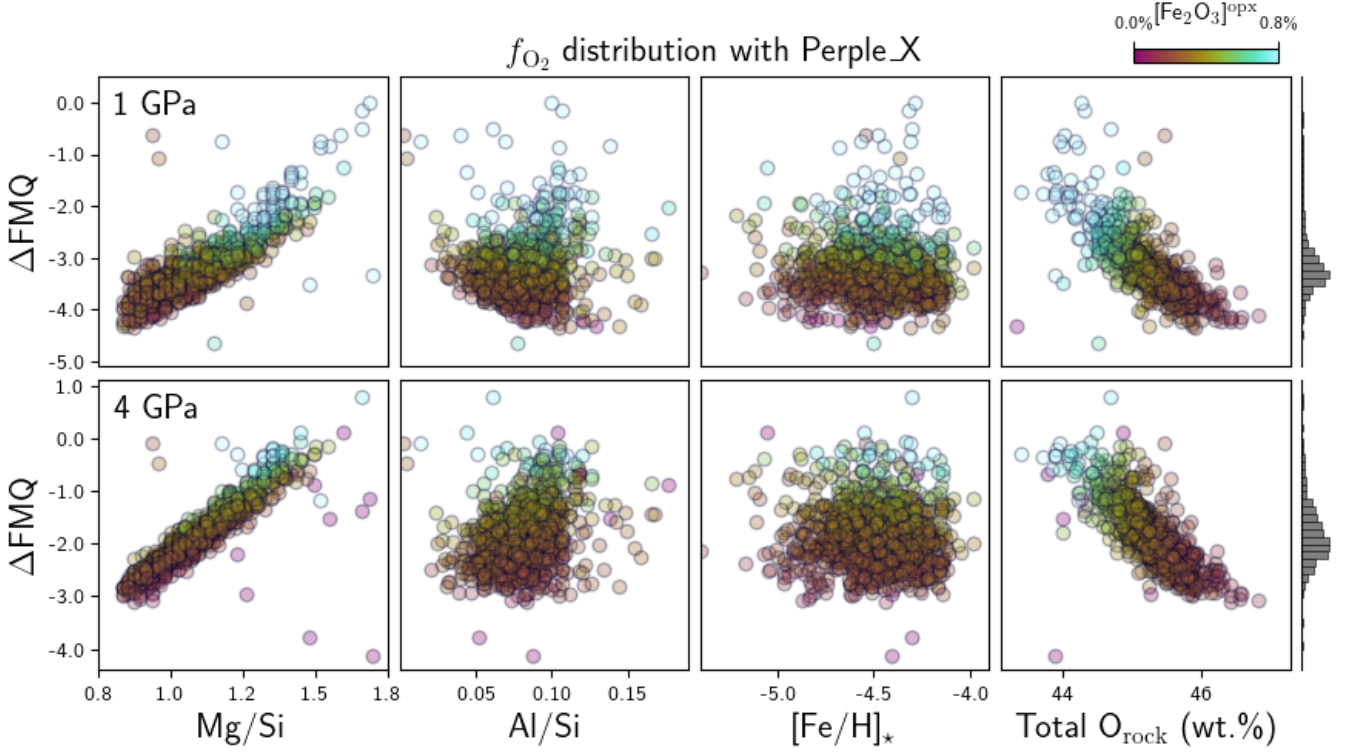


Figure 4. The same results as presented in Figure 3, but using the JH-15 database in Perple_X (and excluding Ti from bulk compositions; $N = 1206$). Note the different y -axis scales.

what we report here if $\text{Fe}^{3+}/\Sigma\text{Fe}$ also varies across exoplanet mantles—empirically true, at the very least, considering Earth and Mars (e.g., Dale et al. 2012). The extent of iron metal core segregation, $\text{Fe}_{\text{mantle}}/(\text{Fe}_{\text{core}} + \text{Fe}_{\text{mantle}})$, could also plausibly affect upper mantle f_{O_2} through its effect on mineralogy. We have therefore calculated exoplanet mantle f_{O_2} distributions as a function of these two key unknown parameters, $\text{Fe}^{3+}/\Sigma\text{Fe}$ and $\text{Fe}_{\text{mantle}}/(\text{Fe}_{\text{core}} + \text{Fe}_{\text{mantle}})$ (Figures 5 and 6 respectively). Here, data in each histogram encompass the same stellar abundance data for known exoplanet host stars (N between 976 and 1232 for pMELTS, and between 1033 and 1251 for JH-15), but varying the fixed parameter $\text{Fe}^{3+}/\Sigma\text{Fe}$ or $\text{Fe}_{\text{mantle}}/(\text{Fe}_{\text{core}} + \text{Fe}_{\text{mantle}})$. We choose generous—yet necessarily arbitrary—ranges for these two parameters, noting that the true upper limits are unknown.

As expected, increasing $\text{Fe}^{3+}/\Sigma\text{Fe}$ means increasing Fe_2O_3 activities and therefore f_{O_2} . Figure 5 shows 2%-increments of $\text{Fe}^{3+}/\Sigma\text{Fe}$: as it increases from 1% to 9%, ΔFMQ increases by about 4 log-units. Yet the widths of the f_{O_2} distributions, represented by their standard deviations, appear similar, $\sigma_{f_{\text{O}_2}} \approx 0.3$ dex at 1 GPa and $\sigma_{f_{\text{O}_2}} \approx 0.4$ dex at 4 GPa. The lack of strong dependence of $\sigma_{f_{\text{O}_2}}$ on (a reasonable range in) Fe oxidation state supports our ability to estimate a minimum f_{O_2} variability. To reiterate, ΔFMQ is unknown so long as we cannot constrain the ferric iron budget of a given exoplanet—the values of $\text{Fe}^{3+}/\Sigma\text{Fe}$ considered here for the purposes of calculation are somewhat arbitrary choices, and larger than the ranges considered in Deng et al. (2020) and Hirschmann (2022) for magma oceans.

All distributions in Figure 5 are wider at 4 GPa compared

to 1 GPa due to the stability of garnet, which generally has higher modality than the lower-pressure aluminous phase spinel, and thus has more scope for affecting Fe^{3+} activities. In detail, distributions are also slightly wider at the lowest Fe^{3+} . The non-linearity of median f_{O_2} versus $\text{Fe}^{3+}/\Sigma\text{Fe}$ is due to the fact that ΔFMQ is logarithmic.

In Figure 6, each histogram now represents a different choice of $\chi_{\text{Fe}}^{\text{mantle}} = \text{Fe}_{\text{mantle}}/(\text{Fe}_{\text{core}} + \text{Fe}_{\text{mantle}})$. Whilst $\text{Fe}^{3+}/\Sigma\text{Fe}$ affects Fe^{3+} activities directly, $\chi_{\text{Fe}}^{\text{mantle}}$ merely changes the wt.% FeO^* of the mantle. Note that no compositions stabilise a Fe-metal phase in the upper mantle, so only FeO and Fe_2O_3 activities are relevant for f_{O_2} (cf. (2): in the much-more-reducing magma ocean, $\chi_{\text{Fe}}^{\text{mantle}}$ is actively linked to f_{O_2} via equilibria between Fe^0 and Fe^{2+}).

Increasing total FeO^* will slightly increase the olivine/orthopyroxene ratio, but otherwise has only a passive influence on f_{O_2} . Figure 6 shows that greater $\chi_{\text{Fe}}^{\text{mantle}}$ means slightly greater f_{O_2} at constant $\text{Fe}^{3+}/\Sigma\text{Fe}$, which is explained by this stabilising effect of FeO^* on olivine, therefore concentrating the Fe^{3+} in orthopyroxene (clinopyroxene, spinel, and garnet proportions are unaffected). Again, $\sigma_{f_{\text{O}_2}}$ is similar across the large range of $\chi_{\text{Fe}}^{\text{mantle}}$; these distributions are reliable estimates of minimum f_{O_2} variabilities. The slight row-wise differences in $\sigma_{f_{\text{O}_2}}$ do not follow the same pattern between pressures and thermodynamic datasets, which points to the complex effects of FeO^* on phase stability and resulting Fe^{3+} activities.

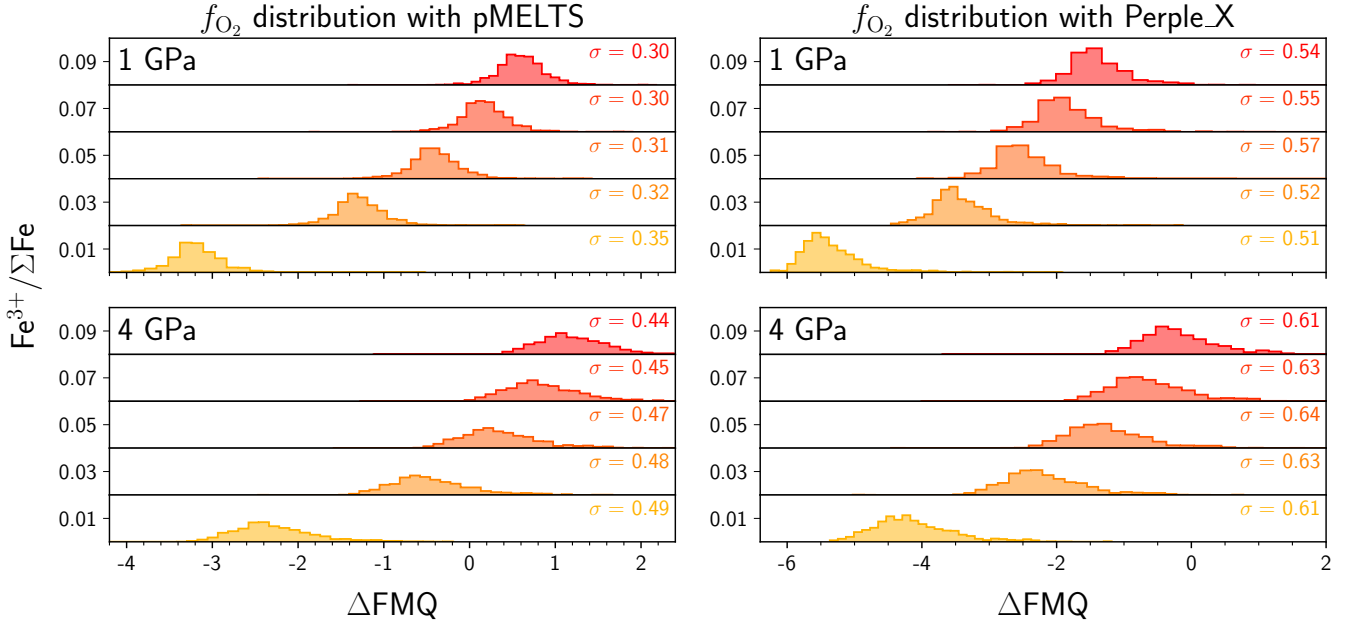


Figure 5. The distributions of mantle oxygen fugacities expressed as ΔFMQ , resulting from chemical variability in Hypatia host stars. Distributions are shown for different mantle $\text{Fe}^{3+}/\Sigma\text{Fe}$ ratios and assuming $\text{Fe}_{\text{mantle}}/(\text{Fe}_{\text{core}} + \text{Fe}_{\text{mantle}}) = 12\%$, at 1 GPa (*top*) or 4 GPa (*bottom*), using the pMELTS (*left*) or JH-15 in Perple_X (*right*) models. Calculations are shown at 1473 K to ensure more compositions have numerically-stable solutions. Standard deviations $\sigma_{f_{\text{O}_2}}$ of each distribution are shown in the upper right corners.

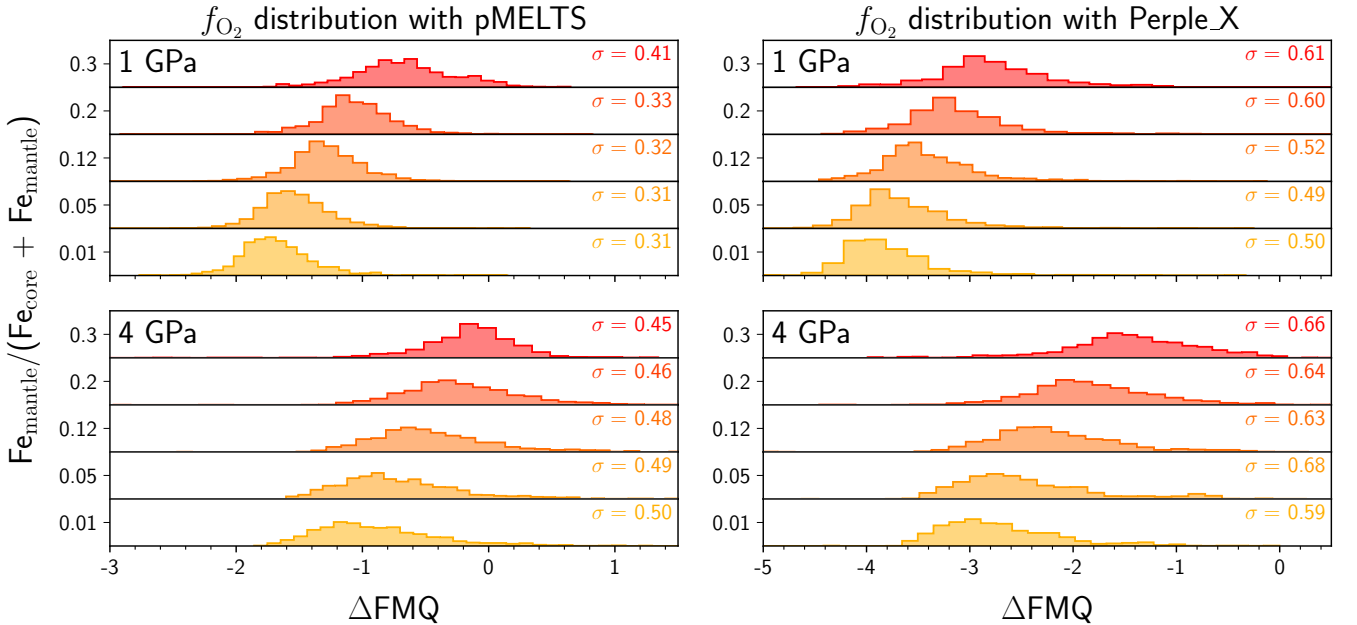


Figure 6. The same as Figure 5, but showing ΔQFM distributions for different choices of $\text{Fe}_{\text{mantle}}/(\text{Fe}_{\text{core}} + \text{Fe}_{\text{mantle}})$, assuming mantle $\text{Fe}^{3+}/\Sigma\text{Fe} = 3\%$. Note the different x -axis scales between models and between here and Figure 5.

3.3.1 Relevance of the core mass fraction for upper mantle f_{O_2}

A final observation from the experiments in Figures 5 and 6 is the relative importance of $\text{Fe}^{3+}/\Sigma\text{Fe}$ and $\chi_{\text{Fe}}^{\text{mantle}}$. Doubling $\text{Fe}^{3+}/\Sigma\text{Fe}$ from an Earth-like value increases the me-

dian ΔFMQ by more than one log-unit; the same ΔFMQ increase would require a much greater change in $\chi_{\text{Fe}}^{\text{mantle}}$. If we compare Figure 6 with Figures 3 and 4, it is clear that the direct effect of stellar abundance variability on exoplanets' upper mantle ΔFMQ is more significant than the direct

effect of the planets' unknown extent of core formation within the range we consider.

That is, the core mass fraction of a planet is not necessarily a proxy for its *upper mantle* f_{O_2} . The equilibrium between Fe-metal and FeO that governs core size is generally no longer operating in the evolved uppermost mantle, if Fe-metal is not present here to buffer electron transfer. The direct relevance of a larger core mass fraction is just to take away from the total mantle iron budget. There are of course indirect effects (beyond the olivine stability mentioned above) in that the physical processes controlling core size may themselves impact the mantle $\text{Fe}^{3+}/\Sigma\text{Fe}$ (that is, $\chi_{\text{Fe}}^{\text{mantle}}$ and $\text{Fe}^{3+}/\Sigma\text{Fe}$ are probably not independent of one another in reality). For example: (i) larger cores come at the expense of high-pressure silicate phases in the lower mantle, phases which may be important for producing Fe^{3+} in planetary interiors; and (ii) certain processes that may affect the mantle Fe^{3+} budget would be more effective at oxidising the mantle when the mantle is more iron-poor, such as H_2O photolysis followed by H_2 loss. These effects are discussed in section 4.2.

4 DISCUSSION

4.1 The effect of mantle f_{O_2} variability on volcanic gas composition and detectability

We choose to focus on one implication of the minimum mantle f_{O_2} variability, the composition of volcanic gas. Light volatile species such as CO_2 and CO , H_2O and H_2 , and SO_2 and H_2S are carried to a planet's surface by magmas, potentially building up volcanic atmospheres (Holland 1962; Gaillard et al. 2021). The speciation of this volcanic gas is controlled by redox reactions and hence f_{O_2} . For example, the two simple equilibria,



will control the relative proportions of H_2 and H_2O and of CO and CO_2 : increasing the availability of O_2 will produce more H_2O and CO_2 at the expense of H_2 and CO . In reality, in atmospheres as in solid mantles, many such equilibria will be operating simultaneously, and the ultimate equilibrium proportions of gas species emerge after considering entire chemical networks.

It is an old paradigm that more-oxidising mantles produce more-oxidising volcanic gas (i.e., the right-hand sides of (9–10)), and more-reducing mantles produce more-reducing volcanic gas (Kasting et al. 1993, and references therein). Magmas plus any gases that exsolve from them would have their net oxidation state and f_{O_2} set in equilibration with their (upper) mantle source region where melting occurs. In detail, once the melt is removed from (no longer buffered by) the mantle, degassing itself may alter the gas oxidation state insofar as certain elements, such as S or C, exchange valence electrons as they transition from the melt phase to the gas phase (e.g., Mathez 1984; Burgisser & Scaillet 2007), although the overall oxidising or reducing power supplied to the surface is unchanged. In the following calculations, we nevertheless make the simplifying assumption that the *range* of f_{O_2} for a gas phase in equilibrium with a melt phase is

approximately the same as the (minimum) *range* of f_{O_2} for upper mantles which we have calculated in section 3.

4.1.1 Calculation of outgassed mixing ratios

As an indication of how intrinsic variability in a planet's upper mantle f_{O_2} may impact its atmospheric chemistry, we use FastChem (Kitzmann & Stock 2018; Stock et al. 2022) to calculate gas phase mixing ratios (the number of moles of a gas phase per total moles of air) as a function of f_{O_2} . FastChem uses Gibbs free energy minimisation to obtain the equilibrium speciation of a gas from input elemental ratios. In this investigation, we focus on gases containing volatile C–O–S–H species only.

The f_{O_2} of a mixture of gas without any condensate is defined simply by the O_2 mixing ratio. The input elemental oxygen abundance that will produce a C–O–S–H gas mixture with the desired absolute f_{O_2} value at a given pressure and temperature is not known *a priori*, but must be found by varying the input elemental abundances. Keeping all elemental abundances fixed and varying only the relative O abundance, we obtain the elemental composition that produces a gas mixture at a desired f_{O_2} . For our choice of input elemental abundances, we choose two sets of values: (i) solar C–S–H ratios, to represent a primordial gas composition; and (ii) Venusian atmospheric C–S–H ratios, to represent a volcanic gas composition. We then run FastChem through a linear bisection algorithm that varies the relative elemental O abundance for each set of input elemental ratios until the target f_{O_2} is output. This determines the gas speciation of volatiles of interest in two atmospheric types, a primordial atmosphere and a volcanically-derived atmosphere, where in both cases the redox chemistry has been set by upper mantle f_{O_2} .

How much the mixing ratio of a species will change with f_{O_2} depends on where the system is located in f_{O_2} -space. For example, in a simple C–O system (10), the shift from CO-dominated to CO_2 -dominated speciation occurs around $\Delta\text{FMQ} - 2$; above this point there is little subsequent variation in X_{CO_2} . Therefore, in addition to the two scenarios of elemental abundances, we also consider two nominal scenarios for where the mantle f_{O_2} distribution is centred: (i) at $\text{IW} - 2$, representing Earth's early reduced mantle at the time of core formation; and (ii) at FMQ, representing Earth's evolved, oxidised upper mantle.

To obtain a volcanic gas mixing ratio distribution, we re-centre the mean of the pMELTS f_{O_2} distribution (Figure 3) on FMQ and on $\text{IW} - 2$, to obtain two sets of f_{O_2} distributions each for the primordial and volcanic compositions. Re-centering is approximately equivalent to changing the wt.% composition of O_2 or the mantle $\text{Fe}^{3+}/\Sigma\text{Fe}$. We use the f_{O_2} distribution at 4 GPa to reflect the mantle source under a thick stagnant lid (Noack et al. 2017; Gaillard et al. 2021, see section 2.1.1), representing a prototypical rocky planet (Stern et al. 2018). For each f_{O_2} value in the distribution, we run FastChem in 0D, at 1 bar and 800 K to obtain the equilibrium composition of a hypothetical gas outgassed at the planet's surface. We emphasise that these calculations express the equilibrium mixing ratios of the gas *input* to the atmosphere for constant C–O–S–H gas composition; we do not model further processing in the atmosphere such as pho-

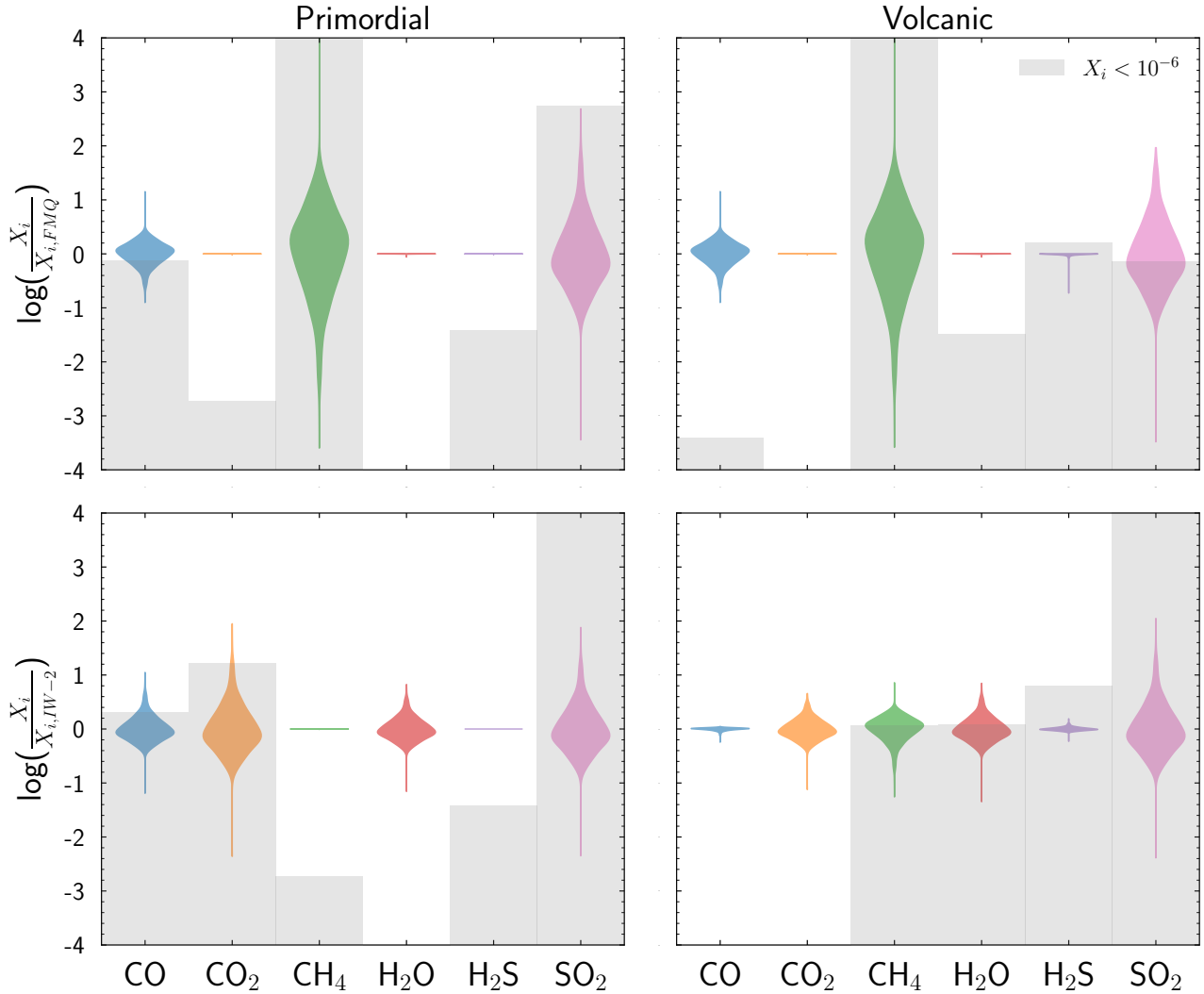


Figure 7. Violin plots of the variation in volcanic gas speciation resulting from our calculated mantle f_{O_2} variability. Speciation is expressed on the y -axis as the the mixing ratio X at the calculated f_{O_2} , relative to what the mixing ratio would be at a reference f_{O_2} —either FMQ (modern Earth’s upper mantle; *top*) or IW – 2 (Earth’s mantle at core formation; *bottom*)—with distributions normalised such that the median f_{O_2} is that of the reference. Distributions are shown for two nominal bulk atmosphere C-S-H ratios: a primordial composition (*left*) reflecting the protoplanetary disk, and a volcanic composition (*right*) reflecting Venus’ present-day atmosphere. The grey patches show where mixing ratios are less than 1 ppm and therefore likely below the detection limit in an exoplanet atmosphere. This example calculation uses our f_{O_2} distribution from pMELTS at 4 GPa (nominally representative of melting below a stagnant lid), projected to a degassing temperature and pressure of 800 K and 1 bar.

tochemistry, equilibration with an ocean or crust, etc., nor do we model the solubility of these species in the melt.

Figure 7 shows the resulting variation in the abundances of the volcanic gases CO, CO₂, CH₄, H₂O, H₂S and SO₂, which can be up to tenfold due essentially to mantle Mg/Si (i.e., the first-order driver of mineralogy in the magma source region). This figure can demonstrate when the mantle f_{O_2} minimum variability affects the composition and detectability of volcanic gas species in exoplanet atmospheres. In many cases, all mixing ratios remain below a nominal 1 ppm detection limit, but there are mentionable exceptions.

For carbon species, mineralogical f_{O_2} modulation has order-of-magnitude effects on CO₂ and CH₄ mixing ratios, and can modulate CH₄ from undetectable to detectable in reduced volcanic atmospheres—notable, given CH₄’s possible

service as a biosignature gas (e.g., Wogan et al. 2020). Detectable outgassed CO mixing ratios can change by several-fold due to mantle Mg/Si variations, even with a moderately oxidising Fe redox state in the upper mantle.

For sulphur species, there is clearly a large effect of mantle Mg/Si on the directly-outgassed mixing ratio of SO₂ in all four scenarios, all else equal. This effect may be enough to raise outgassed SO₂ above a nominal detection threshold in an oxidised volcanic atmosphere. Potentially large changes in directly-outgassed SO₂ mixing ratios, even at very trace, undetectable absolute amounts, may still be consequential for photochemistry and aerosol formation, and their associated effects (e.g., Loftus et al. 2019; Jordan et al. 2021).

Finally, Figure 7 shows that nominally-detectable amounts of H₂O might be outgassed from an upper mantle with a

“reduced” Fe redox state, for the upper half of the Mg/Si distribution.

Whilst the calculations in Figure 7 were performed at a nominal 1 bar and 800 K, different pressures or temperatures affect the volcanic gas chemistry. Pressure variations from 0.1 to 10 bar generally have minor effects on the shapes of the mixing ratio distributions, but do affect the overall abundance of certain species and so their detectability, namely CO and CO₂ in primordial atmospheres and CH₄ and H₂O in volcanic atmospheres (Supplementary Figures S3–S4), in addition to pressure’s solubility effects mentioned below. The trends with temperature are more variable, and species that straddle our potentially observable boundary switch with changing temperature from 600 to 1000 K (Supplementary Figures S5–S6). More detailed studies of exoplanet outgassing would treat atmospheric pressure and temperature sensitively.

4.1.2 Other consequences of f_{O_2} on mantle outgassing: mantle-melt partitioning and gas solubility

Some oxidised species appear to be much more soluble in basaltic melts than reduced counterparts; for example, H₂O vs. H₂, and CO₂ vs. CO and CH₄ (Gaillard & Scaillet 2014, and references therein). At ~ 1 bar we can assume most of these volatiles do degas, but at Venus-like atmospheric pressures (= magma degassing pressures), the higher solubilities of these oxidised species will limit their tendency to degas from the magma. Further, the fraction of S that degasses from a basaltic melt even at 1 bar has a strong positive correlation with f_{O_2} below FMQ, which would amplify the SO₂ variability in Figure 7 (Gaillard et al. 2015, and references therein). These phenomena point to a general effect of f_{O_2} on the total mass of volatiles outgassed—depending on the atmospheric pressure—which compounds the effect of f_{O_2} on gas phase speciation.

In a similar phenomenon, the movement of carbon from the solid mantle into partial melt may be limited at f_{O_2} below IW, where carbon takes the form of graphite (Holloway et al. 1992; Holloway 1998; Grott et al. 2011; Wetzel et al. 2013; Armstrong et al. 2015; Li et al. 2017). Therefore, at modest atmospheric pressures, the less-efficient extraction of carbon from such reduced mantles could limit the total mass of carbon species they can outgas, all else equal (Guimond et al. 2021).

4.2 Some reasons for planet-planet $\text{Fe}^{3+}/\Sigma\text{Fe}$ variability

Whilst we have calculated the distributions of ΔFMQ across a naïve range of fixed $\text{Fe}^{3+}/\Sigma\text{Fe}$ values (Figure 5), the true underlying distribution of $\text{Fe}^{3+}/\Sigma\text{Fe}$ is unknown. Below are several ways whereby Fe^{3+} could be produced in planetary interiors, each implying different upper limits on $\text{Fe}^{3+}/\Sigma\text{Fe}$:

(i) Endogenous processes

(a) *Iron disproportionation*—The crystallisation of perovskite from the magma ocean triggers a reaction where FeO disproportionates into Fe-metal plus Fe₂O₃ (see section 1.1). Fe₂O₃ stabilises perovskite, whilst Fe-metal likely sinks to the growing core. This process, sometimes called

mantle self-oxidation, can occur on planets large enough to reach perovskite stability pressures (e.g., Frost et al. 2004; Wade & Wood 2005; Wood et al. 2006; Frost & McCammon 2008). Hence self-oxidation (or lack thereof) has been put forward as a reason why Mars’ mantle appears more reducing than Earth’s—Mars’ mantle is too shallow to stabilise perovskite (Wade & Wood 2005). The amount of Fe³⁺ that can be produced by disproportionation is hard-limited by the total amount of Fe in perovskite (plus postperovskite; Catalli et al. 2010). Deeper mantles would produce more Fe³⁺, which may then be slowly homogenised in the mantle through solid-state convection. However, if Fe-metal *does not* sink to the core, which may be the case on the most massive rocky planets due to their turbulent magma oceans (Lichtenberg 2021), then there is not necessarily a continuous trend between the size of a planet and how oxidised its mantle is.

(b) *Pressure-dependent Fe³⁺ stability in the magma ocean*—Higher pressures increasingly favour Fe³⁺ over Fe²⁺ in molten silicates, due to the smaller partial molar volume of the former (Kress & Carmichael 1991; Hirschmann 2012; Armstrong et al. 2019; Deng et al. 2020; Kuwahara et al. 2023). This process is distinct from (i.a) in that it can occur in the magma ocean itself before it crystallises (so Fe³⁺ is more rapidly homogenised). Fe-metal still must be lost to the core in order to effectively oxidise the magma ocean. If the mantle inherits the resulting $\text{Fe}^{3+}/\Sigma\text{Fe}$ of the magma as it crystallises, then deeper magma oceans will also make mantles with higher $\text{Fe}^{3+}/\Sigma\text{Fe}$, due to this Fe³⁺ stability effect. In this way, magma ocean depth may similarly be a principal determinant of overall mantle $\text{Fe}^{3+}/\Sigma\text{Fe}$ (Deng et al. 2020), with the same caveat as in (i.a) of needing Fe-metal to sink.

(c) *Cr oxidation during magma ocean crystallisation*—Because Cr is present as CrO in the deep magma ocean, but as Cr₂O₃ in the solid mantle, CrO may be oxidised during magma ocean crystallisation via the reaction $2\text{CrO} + \text{Fe}_2\text{O}_3 = \text{Cr}_2\text{O}_3 + 2\text{FeO}$, which could decrease $\text{Fe}^{3+}/\Sigma\text{Fe}$ significantly (by a factor of two for Earth) depending on the accreted Cr budget (Hirschmann 2022). This process represents one reason why the mantle $\text{Fe}^{3+}/\Sigma\text{Fe}$ could differ from the magma ocean value.

(ii) Exogenous processes

(a) *Oxidation by volatile accretion*—A substantial layer of volatiles such as H₂O above a magma ocean can be a powerful source of oxidation potential. In this case, the upper limit to how much Fe³⁺ is produced from Fe²⁺ is essentially unconstrained, given unknown initial abundances of volatiles. For example, H₂O dissociation in the atmosphere followed by H₂ escape to space produces O₂, which can then be absorbed by the magma ocean to oxidise FeO into Fe₂O₃. (Schaefer et al. 2016). Similarly, H₂O dissociation in a magma ocean produces H₂ and Fe₂O₃; the H₂ degasses, increasing $\text{Fe}^{3+}/\Sigma\text{Fe}$ of the magma ocean (Sharp et al. 2013; Sharp 2017). After the magma ocean crystallises, the early crust could also be a sink for atmospheric free oxygen—which, if subducted or otherwise buried, could also contribute to mantle oxidation (e.g., Krissansen-Totton et al. 2021). Late accretion of Fe³⁺-rich chondritic material has also been proposed to have oxidised Earth’s mantle (O’Neill 1991). Meanwhile, metal-rich en-

statite chondritic material or even organic C in carbonaceous chondritic material could plausibly cancel out this oxidising power (Hirschmann 2022).

4.3 The underlying rocky planet Mg/Si distribution?

Mantle compositions will only represent host star refractory element abundances if no additional processes partition these elements relative to one another whilst planets form and differentiate. However, several processes may increase Mg/Si relative to the primordial protoplanetary disk (Ringwood 1989; Trønnes et al. 2019; Miyazaki & Korenaga 2020). A salient example is that the Sun’s composition produces an Mg/Si ratio of 1.05, yet measurements of Earth mantle xenoliths suggest Mg/Si \approx 1.24 (the bulk mantle may not be well-represented by these upper mantle xenoliths; Javoy 1995). A small systematic offset in bulk planet Mg/Si would manifest as a small translation of the f_{O_2} distribution. Since our model merely captures the effect of Mg/Si variation on f_{O_2} , it is agnostic to what actually causes this variation (e.g., stellar abundances alone, or stellar abundances plus secondary processes). Because it seems unlikely that secondary processes would converge to *decrease* the amount of inter-planet Mg/Si variation, our reported f_{O_2} variability remains a minimum. Although our results are therefore not strictly sensitive to the true median of the Mg/Si distribution of rocky planets, it is worth briefly discussing the degree to which a planet’s Mg/Si might be modulated away from its host star. Because mantles with Mg/Si approximately $\in [0.7, 1.5]$ will have pyrolytic (i.e., pyroxene- and olivine-dominated) compositions (Guimond et al. 2023), a median Mg/Si offset of at least -0.3 or $+0.5$ is necessary to significantly alter the mineralogically-derived spread in f_{O_2} .

Some Si likely enters the metal core (e.g., Ringwood 1959; Javoy 1995; Wood et al. 2006; Schaefer et al. 2017). On an Earth mass planet, partitioning Si into a metal core such that the core is 15 wt.% Si, 32.5% of the planet mass, and contains 88% of the planet’s iron atoms would increase a “solar-derived” mantle Mg/Si to 1.42, for example. We choose to not explicitly model metal/silicate Si partitioning—i.e., Fe is the only element modified by planetary differentiation—in order to avoid unconstrained and unnecessary complexity. In particular, the value of the metal/silicate partitioning coefficient depends on the temperature and pressure conditions at the base of the magma ocean. However, if Si decreasingly partitions into metal at higher pressures (Schaefer et al. 2017), then more massive planets may evolve upper mantles which are systematically slightly pyroxene-richer, and thus more reduced.

4.3.1 Oxygen fugacity of silica-saturated mantles

Although we excluded compositions from our results which stabilise pure SiO_2 phases, these mineralogies could exist at mantle Mg/Si $\lesssim 0.7$ (or $\sim 6\%$ of the Hypatia stars in our sample), depending on the mantle FeO^* content. Silica-saturated mineralogies have a distinct pattern of f_{O_2} : when they exist, we find a composition-independent f_{O_2} , consistently about 2 log-units higher than the median for the given $\text{Fe}^{3+}/\Sigma\text{Fe}$. However, the thermodynamic data is not well-constrained

here, and more experiments are needed to understand these hypothetical exotic mantle mineralogies.

4.4 Limitations due to thermodynamic data

In working with the two models JH-15 and pMELTS, our results naturally inherit their limitations. In particular, the thermodynamic activities determined by these datasets and solution models are not necessarily applicable to the wide range of exoplanet compositions that we consider here, and the associated caveats apply to our results. As an example, the models assume olivine is Fe^{3+} -free under all conditions. Even in the compositional ranges for which they were developed, the two models contain different assumptions: Perple_X includes Fe^{3+} in its garnet solution model, whilst pMELTS does not (Figure 2).

On the basis of their similar spreads of f_{O_2} (despite dissimilarities like that with the garnet model), we have nevertheless argued that a minimum f_{O_2} variability is robust. Importantly, both models include ferric iron in pyroxene: this is a key reservoir for determining how oxidising a planet’s source of magmatism is. However, the partitioning of Fe^{3+} between pyroxene and melts is poorly constrained experimentally (although there have been recent attempts; Rudra et al. 2021). Thus future models, informed by new experiments, may differ particularly in how mantle f_{O_2} evolves during progressive melting. In sum, we anticipate that more experiments in the near future, based in experimental petrology or first-principles molecular dynamics, would extend the reliable thermodynamic data into the wider—yet likely finite—compositional space of rocky planet mantles.

5 CONCLUSIONS

This work has identified a tractable component of the f_{O_2} distribution across exoplanet mantles: we have calculated the minimum width of the distributions due to mineral phase equilibria at 1 and 4 GPa. The actual centre (and to a lesser extent the true width) of the distribution remains unknown unless we know what ratios of Fe^{3+} to Fe^{2+} to expect for these planets. Nevertheless, we find similar f_{O_2} standard deviations for widely variable values of mantle $\text{Fe}^{3+}/\Sigma\text{Fe}$, pointing to a robust minimum f_{O_2} variability that ultimately reflects the measured refractory element distribution across >1000 host stars from the Hypatia Catalog.

Whilst $\text{Fe}^{3+}/\Sigma\text{Fe}$ might be said to set the bulk oxidation state of the upper mantle—Fe is by far the most abundant multivalent rock-forming element—the relationship between $\text{Fe}^{3+}/\Sigma\text{Fe}$ and f_{O_2} is not unique because the various mineral equilibria controlling f_{O_2} will also shift with bulk composition (Frost 1991). We have demonstrated this fact by finding a wide range of absolute f_{O_2} for planets with identical $\text{Fe}^{3+}/\Sigma\text{Fe}$ but plausibly different proportions of olivine, pyroxene, and spinel or garnet.

In particular, we show that a planetary mantle’s Mg/Si ratio alone has an order-of-magnitude effect on the f_{O_2} of its upper mantle. This effect is comparable to the effect on upper mantle f_{O_2} of decreasing FeO^* by locking Fe metal in the core. Mg/Si controls the relative proportions of the abundant minerals olivine and pyroxenes; since pyroxenes can incorporate Fe^{3+} in their crystal structures but olivine cannot,

increasing pyroxene proportions with decreasing Mg/Si will dilute (lower the activity of) the Fe^{3+} -bearing component in pyroxenes, hence lowering the f_{O_2} of the system (Stolper et al. 2020). This effect induces compositional variability in mantle f_{O_2} across rocky planets.

To illustrate one planetary consequence of this mantle f_{O_2} variability, we predict the distributions in volcanic gas composition that directly result from our f_{O_2} distribution, given that the f_{O_2} of these mantle-derived gases inherits the f_{O_2} of the mantle source region (e.g., Gaillard et al. 2015). Depending on the C-H-S ratio and median f_{O_2} , the resulting mixing ratios of outgassed CO , CH_4 , and SO_2 can differ by up to ten-fold, due to mantle mineralogy variations alone. Overall, our results establish another role for mantle composition to play in the detectability of atmospheric species on rocky worlds and in quantifying abiotic baselines for interpreting biosignatures.

ACKNOWLEDGEMENTS

We acknowledge the support of the University of Cambridge Harding Distinguished Postgraduate Scholars Programme and the Natural Sciences and Engineering Research Council of Canada (NSERC). Cette recherche a été financée par le Conseil de recherches en sciences naturelles et ingénierie du Canada (CRSNG). The research shown here acknowledges use of the Hypatia Catalog Database, an online compilation of stellar abundance data as described in Hinkel et al. (2014, *AJ*, 148, 54), which was supported by NASA’s Nexus for Exoplanet System Science (NExSS) research coordination network and the Vanderbilt Initiative in Data-Intensive Astrophysics (VIDA). This manuscript has benefitted from a thoughtful review by Jie Deng, as well as from discussions with Amy Bonsor and Sami Mikhail.

DATA AVAILABILITY

The Python code and the pMELTS and Perple_X input files used in this study are available from the authors upon request.

References

Anders E., Ebihara M., 1982, *Geochimica et Cosmochimica Acta*, 46, 2363

Armstrong L. S., Hirschmann M. M., Stanley B. D., Falken E. G., Jacobsen S. D., 2015, *Geochimica et Cosmochimica Acta*, 171, 283

Armstrong K., Frost D. J., McCammon C. A., Rubie D. C., Boffa Ballaran T., 2019, *Science*, 365, 903

Asimow P. D., Giorso M. S., 1998, *American Mineralogist*, 83, 1127

Ballhaus C., 1995, *Earth and Planetary Science Letters*, 132, 75

Bonsor A., Jofré P., Shorttle O., Rogers L. K., Xu S., Melis C., 2021, *Monthly Notices of the Royal Astronomical Society*, 503, 1877

Brouwers M. G., Buchan A. M., Bonsor A., Malamud U., Lynch E., Rogers L., Koester D., 2023, *Monthly Notices of the Royal Astronomical Society*, 519, 2663

Burgisser A., Scaillet B., 2007, *Nature*, 445, 194

Catalli K., Shim S. H., Prakapenka V. B., Zhao J., Sturhahn W., 2010, *American Mineralogist*, 95, 418

Connolly J. a. D., 2009, *Geochemistry, Geophysics, Geosystems*, 10

Dale C. W., Burton K. W., Greenwood R. C., Gannoun A., Wade J., Wood B. J., Pearson D. G., 2012, *Science*, 336, 72

Delano J. W., 2001, *Origins of life and evolution of the biosphere*, 31, 311

Deng J., Du Z., Karki B. B., Ghosh D. B., Lee K. K. M., 2020, *Nature Communications*, 11, 2007

Dorn C., Khan A., Heng K., Alibert Y., Connolly J. A. D., Benz W., Tackley P., 2015, *Astronomy & Astrophysics*, 577, A83

Dorn C., Venturini J., Khan A., Heng K., Alibert Y., Helled R., Rivoldini A., Benz W., 2017a, *Astronomy & Astrophysics*, 597, A37

Dorn C., Hinkel N. R., Venturini J., 2017b, *Astronomy and Astrophysics*, 597, A38

Dorn C., Harrison J. H. D., Bonsor A., Hands T. O., 2019, *Monthly Notices of the Royal Astronomical Society*, 484, 712

Doyle A. E., Young E. D., Klein B., Zuckerman B., Schlichting H. E., 2019, *Science*, 366, 356

Doyle A. E., Klein B., Schlichting H. E., Young E. D., 2020, *The Astrophysical Journal*, 901, 10

Doyle A. E., et al., 2023, New Chondritic Bodies Identified in Eight Oxygen-Bearing White Dwarfs (arxiv:2303.00063)

Elkins-Tanton L. T., Seager S., 2008, *The Astrophysical Journal*, 688, 628

Foley S. F., 2011, *Journal of Petrology*, 52, 1363

Frost B. R., 1991, *Reviews in Mineralogy and Geochemistry*, 25, 1

Frost D. J., McCammon C. A., 2008, *Annual Review of Earth and Planetary Sciences*, 36, 389

Frost D. J., Lieske C., Langenhorst F., McCammon C. A., Trønnes R. G., Rubie D. C., 2004, *Nature*, 428, 409

Gaillard F., Scaillet B., 2014, *Earth and Planetary Science Letters*, 403, 307

Gaillard F., Scaillet B., Pichavant M., Iacono-Marziano G., 2015, *Chemical Geology*, 418, 217

Gaillard F., et al., 2021, *Space Science Reviews*, 217, 22

Giorso M. S., Hirschmann M. M., Reiners P. W., Kress III V. C., 2002, *Geochemistry, Geophysics, Geosystems*, 3, 1

Grott M., Morschhauser A., Breuer D., Hauber E., 2011, *Earth and Planetary Science Letters*, 308, 391

Guimond C. M., Noack L., Ortenzi G., Sohl F., 2021, *Physics of the Earth and Planetary Interiors*, 320, 106788

Guimond C. M., Shorttle O., Rudge J. F., 2023, *Monthly Notices of the Royal Astronomical Society*, 521, 2535

Hinkel N. R., Unterborn C. T., 2018, *The Astrophysical Journal*, 853, 83

Hinkel N. R., Timmes F. X., Young P. A., Pagano M. D., Turnbull M. C., 2014, *The Astronomical Journal*, 148, 54

Hirschmann M. M., 2012, *Earth and Planetary Science Letters*, 341–344, 48

Hirschmann M. M., 2022, *Geochimica et Cosmochimica Acta*, 328, 221

Holland H. D., 1962, in Engel A. E. J., James H. L., Leonard B. F., eds., *Petrologic Studies*. Geological Society of America, p. 0, doi:10.1130/Petrologic.1962.447

Holland H. D., 2002, *Geochimica et Cosmochimica Acta*, 66, 3811

Holloway J., 1998, *Chemical Geology*, 147, 89

Holloway J., Pan V., Gudmundsson G., 1992, *European Journal of Mineralogy*, 4, 105

Javoy M., 1995, *Geophysical Research Letters*, 22, 2219

Jennings E. S., Holland T. J. B., 2015, *Journal of Petrology*, 56, 869

Jordan S., Rimmer P. B., Shorttle O., Constantinou T., 2021, *The Astrophysical Journal*, 922, 44

Kasting J. F., Catling D., 2003, *Annual Review of Astronomy and Astrophysics*, 41, 429

- Kasting J. F., Egger D. H., Raeburn S. P., 1993, *The Journal of Geology*, 101, 245
- Kitzmann D., Stock J., 2018, *Astrophysics Source Code Library*, p. ascl:1804.025
- Kress V. C., Carmichael I. S. E., 1991, *Contributions to Mineralogy and Petrology*, 108, 82
- Krissansen-Totton J., Fortney J. J., Nimmo F., Wogan N., 2021, *AGU Advances*, 2, e2020AV000294
- Krissansen-Totton J., Thompson M., Galloway M. L., Fortney J. J., 2022, *Nature Astronomy*, 6, 189
- Kuwahara H., Nakada R., Kadoya S., Yoshino T., Irifune T., 2023, *Nature Geoscience*, 16, 461
- Li Y., Dasgupta R., Tsuno K., 2017, *Journal of Geophysical Research: Planets*, 122, 1300
- Lichtenberg T., 2021, arXiv:2105.11208 [astro-ph, physics:physics]
- Liggins P., Shorttle O., Rimmer P. B., 2020, *Earth and Planetary Science Letters*, 550, 116546
- Liggins P., Jordan S., Rimmer P. B., Shorttle O., 2022, *Journal of Geophysical Research: Planets*, 127, e2021JE007123
- Lin Y., van Westrenen W., Mao H.-K., 2021, *Proceedings of the National Academy of Sciences*, 118, e21110427118
- Lodders K., Palme H., Gail H. P., 2009, *Landolt Börnstein*, 4B, 712
- Loftus K., Wordsworth R. D., Morley C. V., 2019, *The Astrophysical Journal*, 887, 231
- Mathez E. A., 1984, *Nature*, 310, 371
- Miyazaki Y., Korenaga J., 2020, arXiv:2004.13911 [astro-ph, physics:physics]
- Muchowska K. B., Varma S. J., Moran J., 2019, *Nature*, 569, 104
- Noack L., Rivoldini A., Van Hoolst T., 2017, *Physics of the Earth and Planetary Interiors*, 269, 40
- O'Neill H., 1991, *Geochimica et Cosmochimica Acta*, 55, 1159
- O'Neill H. St.C., Rubie D. C., Canil D., Geiger C. A., Ross II C. R., Seifert F., Woodland A. B., 1993, in , *Evolution of the Earth and Planets*. American Geophysical Union (AGU), pp 73–88, doi:10.1029/GM074p0073
- Ortenzi G., et al., 2020, *Scientific Reports*, 10, 10907
- Otegi J. F., Dorn C., Helled R., Bouchy F., Haldemann J., Alibert Y., 2020, *Astronomy and Astrophysics*, 640, A135
- Putirka K. D., Rarick J. C., 2019, *American Mineralogist*, 104, 817
- Righter K., Ghiorso M. S., 2012, *Proceedings of the National Academy of Sciences*, 109, 11955
- Ringwood A. E., 1959, *Geochimica et Cosmochimica Acta*, 15, 257
- Ringwood A. E., 1989, *Earth and Planetary Science Letters*, 95, 1
- Rohrbach A., Ballhaus C., Golla-Schindler U., Ulmer P., Kamenetsky V. S., Kuzmin D. V., 2007, *Nature*, 449, 456
- Rubie D. C., et al., 2015, *Icarus*, 248, 89
- Rudra A., Cottrell E., Hirschmann M. M., 2021, *Chemical Geology*, 584, 120532
- Santos N. C., et al., 2017, *Astronomy & Astrophysics*, 608, A94
- Schaefer L., Wordsworth R. D., Berta-Thompson Z., Sasselov D., 2016, *The Astrophysical Journal*, 829, 63
- Schaefer L., Jacobsen S. B., Remo J. L., Petaev M. I., Sasselov D. D., 2017, *The Astrophysical Journal*, 835, 234
- Sharp Z. D., 2017, *Chemical Geology*, 448, 137
- Sharp Z. D., McCubbin F. M., Shearer C. K., 2013, *Earth and Planetary Science Letters*, 380, 88
- Spaargaren R. J., Ballmer M. D., Bower D. J., Dorn C., Tackley P. J., 2020, *Astronomy & Astrophysics*, 643, A44
- Spaargaren R. J., Wang H. S., Mojzsis S. J., Ballmer M. D., Tackley P. J., 2023, *ApJ*, 948, 53
- Stagno V., Ojwang D. O., McCammon C. A., Frost D. J., 2013, *Nature*, 493, 84
- Stähler S. C., et al., 2021, *Science*
- Stern R. J., Gerya T., Tackley P. J., 2018, *Geoscience Frontiers*, 9, 103
- Stock J. W., Kitzmann D., Patzer A. B. C., 2022, *Monthly Notices of the Royal Astronomical Society*, p. stac2623
- Stolper E. M., Shorttle O., Antoshechkina P. M., Asimow P. D., 2020, *American Mineralogist*, 105, 1445
- Thiabaud A., Marboeuf U., Alibert Y., Leya I., Mezger K., 2015, *Astronomy & Astrophysics*, 580, A30
- Trønnes R. G., Baron M. A., Eigenmann K. R., Guren M. G., Heyn B. H., Løken A., Mohn C. E., 2019, *Tectonophysics*, 760, 165
- Unterborn C. T., Panero W. R., 2017, *The Astrophysical Journal*, 845, 61
- Unterborn C. T., Panero W. R., 2019, *Journal of Geophysical Research: Planets*, 124, 1704
- Unterborn C. T., Johnson J. A., Panero W. R., 2015, *The Astrophysical Journal*, 806, 139
- Unterborn C. T., Foley B. J., Desch S. J., Young P. A., Vance G., Chiffelle L., Kane S. R., 2022, *The Astrophysical Journal Letters*, 930, L6
- Unterborn C. T., Desch S. J., Haldemann J., Lorenzo A., Schulze J. G., Hinkel N. R., Panero W. R., 2023, *The Astrophysical Journal*, 944, 42
- Wade J., Wood B. J., 2005, *Earth and Planetary Science Letters*, 236, 78
- Wade J., Byrne D. J., Ballentine C. J., Drakesmith H., 2021, *Proceedings of the National Academy of Science*, 118, e2109865118
- Wang H. S., Liu F., Ireland T. R., Brasser R., Yong D., Lineweaver C. H., 2019, *Monthly Notices of the Royal Astronomical Society*, 482, 2222
- Wang H. S., Quanz S. P., Yong D., Liu F., Seidler F., Acuña L., Mojzsis S. J., 2022, *Monthly Notices of the Royal Astronomical Society*
- Wetzel D. T., Rutherford M. J., Jacobsen S. D., Hauri E. H., Saal A. E., 2013, *Proceedings of the National Academy of Sciences*, 110, 8010
- Williams H. M., Wood B. J., Wade J., Frost D. J., Tuff J., 2012, *Earth and Planetary Science Letters*, 321–322, 54
- Wogan N., Krissansen-Totton J., Catling D. C., 2020, *The Planetary Science Journal*, 1, 58
- Wood B. J., Walter M. J., Wade J., 2006, *Nature*, 441, 825
- Wordsworth R. D., Schaefer L. K., Fischer R. A., 2018, *The Astronomical Journal*, 155, 195
- Workman R. K., Hart S. R., 2005, *Earth and Planetary Science Letters*, 231, 53